A Shallow-Water Model of the Diurnal Dryline

JENNIFER A. MILLER, THOMAS A. KOVACS, AND PETER R. BANNON

Department of Meteorology, The Pennsylvania State University, University Park, Pennsylvania

(Manuscript received 21 July 2000, in final form 8 February 2001)

ABSTRACT

This study explores the diurnal variation in the movement and structure of the dryline using a one-dimensional shallow-water model. The model is adapted to test some common theories of dryline motion including the diurnal variation in surface friction, static stability, inversion erosion, and momentum mixing aloft.

These mechanisms of diurnal variation are first studied individually and then in unison. A diurnal variation in the surface friction produces a model dryline that moves westward during the day (in disagreement with observations) and has a southerly wind maximum near midnight. A diurnal variation in the static stability produces a model dryline that steepens in slope and moves eastward during the day and then surges westward at night with a southerly wind maximum 6 to 9 h after the minimum stability. Inversion erosion during the day produces a nearly vertical model dry front that moves eastward during the day with surface southwesterlies. At sunset the model dryline surges westward with a southerly wind maximum before midnight. A diurnal variation of the momentum mixing aloft has no significant effect on the model dryline. Results show that the combined case with a diurnal variation of surface friction, inversion erosion, and static stability with terrain most accurately describes the observed dryline system. The westward surge depicted in the model is compared to the flow evolution of the corresponding dam-break problem for a rotating fluid.

1. Introduction

The dryline is the surface boundary between cool moist maritime air from the Gulf of Mexico and warm dry continental air from the desert interior of North America, and is a preferred location for the development of thunderstorms over the Great Plains. In a climatological study Rhea (1966) finds that, when a dryline is present, the first new radar echoes of the day develop within 40 km of the dryline about 78% of the time. Usually the echoes form to the east of the dryline. In case studies Bluestein et al. (1988) describe a tornadic storm near a dryline while Bluestein and Parker (1993) discuss the modes of severe weather along the dryline. Sun (1987) and Hane et al. (1993) also emphasize the link between severe weather and the dryline.

The quiescent dryline exhibits a diurnal variation. By quiescent we mean the prestorm environment in the absence of major synoptic-scale forcing. The dryline progresses eastward during the late morning and early afternoon, and it retrogresses westward in the late evening and overnight (Schaefer 1986). The eastward progression is typically much larger than the retrogression, resulting in a net eastward progression. The slope of the airmass boundary is small at night and in the early morning (Sun and Wu 1992), but becomes nearly vertical by the afternoon (e.g., Fujita 1958; Ziegler and Rasmussen 1998). In one case, Ziegler and Rasmussen (1998) observe that the leading edge of the dryline was quasi-vertical and almost stationary several hours after sunrise. The moisture gradient can be diffuse at night and in the early morning, but is typically well defined in the afternoon (Schaefer 1986).

This paper presents a theoretical modeling study of the quiescent dryline. The next section reviews the observational, theoretical, and modeling studies of the dryline. A conceptual model of the dryline system is presented that includes the dryline, the dry front–lid aloft, and the low-level winds. A number of physical processes including the diurnal variation in surface friction, static stability, inversion erosion, and momentum mixing with the air aloft have been advanced to explain the diurnal evolution of the dryline system. These theories are compared using a one-dimensional shallow-water model. Section 3 describes the model and section 4 presents the model results that assess the various theories of the diurnal variation of the dryline. Section 5 presents a simulation using a combination of physical processes. Section 6 presents our conclusions.

2. A review of the diurnal variation of the dryline system

Schaefer (1986) and Bluestein (1993) review the fundamental features of the dryline. The dryline appears

Corresponding author address: Dr. Peter R. Bannon, Dept. of Meteorology, The Pennsylvania State University, 503 Walker Building, University Park, PA 16802.
E-mail: bannon@ems.psu.edu

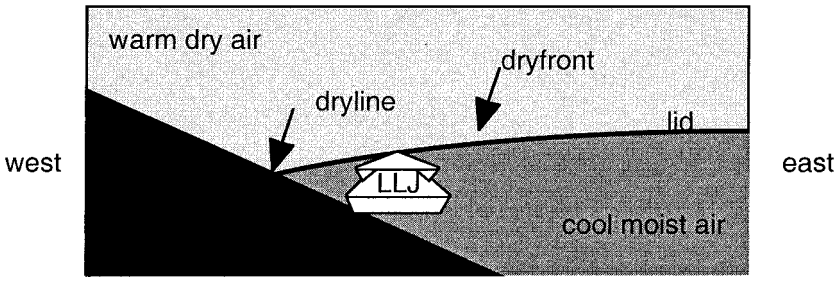

FIG. 1. A schematic diagram of the dryline system consisting of relatively cool moist air separated from warm dry air over the sloping Great Plains by a lid or dry front. The intersection of the dry front with the ground denotes the location of the dryline. Southerly flow in the form of a low-level jet exists in the cool moist air.

on surface maps as a sharp gradient in dewpoint temperature or, equivalently, in the water vapor mixing ratio over the Great Plains. The dryline typically appears about 40% of the time in spring and early summer, the most favorable time of year for severe convection. The dryline runs north to south or southwest to northeast from Texas into Oklahoma and Kansas and occasionally into the Dakotas. The large-scale climatology is one of a low-level confluent pattern between cool moist maritime air from the Gulf of Mexico and warm dry continental air from the interior of North America. This pattern is modified by migratory midlatitude systems (e.g., Hobbs et al. 1996) when a migratory anticyclone strengthens the Bermuda high to the east of the plains while a migratory cyclone lies over the Rocky Mountain massif. This synoptic situation leads to a stronger moisture flux from the Gulf of Mexico. Studies of the synoptic features of the dryline (e.g., Carlson et al. 1980; Djuric and Damiani 1980; Uccellini 1980; Carlson et al. 1983; Djuric and Ladwig 1983; Keyser and Carlson 1984; Lanicci and Warner 1991b; Kaplan and Karyampudi 1992a,b; Chen and Kpaeyeh 1993; Steenburgh and Mass 1994; Martin et al. 1995; Hobbs et al. 1996) are excluded from investigation here and will not be discussed further.

The name ''dryline'' is a misnomer because it is not a line but rather a two-dimensional frontal surface separating the moist and dry air masses. Fujita's (1958) ''dry front'' is perhaps a more accurate description. Here we use the phrase ''dryline system'' to encompass the components of the dryline phenomenon. A schematic west to east cross section with the components of this system appears in Fig. 1. In this perspective the dryline describes the intersection of the dry front with the sloping terrain. It is noted that the moist air is capped by an inversion, nicknamed a ''lid'' by Carlson and Ludlam (1968) to describe its tendency to suppress thunderstorm development even in the presence of large convective available potential energy. The lid is the frontal surface aloft but the dryline is the intersection of the lid with the sloping topography. The moist air below the lid is a convective boundary layer strongly influenced by the diurnal cycle of surface heating. The drier warmer air above the lid is an elevated mixed layer of nearly uniform potential temperature that has advected over the moist air from the west. The climatology of the lid has been documented by Lanicci and Warner (1991a,b,c). Potential temperature differences across the lid are typically about 5 K. The strength of the lid appears to undergo a diurnal variation. Wexler (1961, Fig. 11) shows the lid to be more horizontal at night and more vertical near the dryline during the day. This figure also shows a reduction in the static stability during the day.

The structure of the lid close to the intersection with the sloping terrain has been documented in several aircraft traverses of the dryline during the day. The studies of Fujita (1958), McGuire (1962), NSSP Staff Members (1963), and Ziegler and Hane (1993) show a steep frontal surface with a potential temperature difference of several degrees. McGuire observed essentially no density contrast across a dry front that displayed a vertical tilt. Fujita (1958), Ziegler and Hane (1993), Ziegler and Rasmussen (1998), and Atkins et al. (1998) estimate a frontal slope of about 1:10 or greater. The lidar estimate of Parsons et al. (1991) inferred a slope as large as 1:2. The recent P-3 observations of Ziegler and Hane (1993) reveal a virtual potential temperature difference of about 2 K across the dryline with higher values to the west in the dry air. The bulk of this evidence supports a density contrast across the dryline. Aircraft traverses during the nighttime have not yet been performed but such information is needed to construct the vertical structure of the dry front at night.

It is important to emphasize that the use of surface data to infer the diurnal variation of the density characteristics across the dryline system is misleading. Such data suggest that the horizontal gradient of the virtual potential temperature θ_v reverses diurnally with cooler temperatures to the west of the dryline and warmer temperatures to the east. This reversal is confined only to the depth of the shallow ($\sim$100 m deep) nocturnal inversions and is not indicative of the bulk of the lower atmosphere. Kovacs (1996) examines the diurnal variation in θ_v horizontally across the dryline in a case study. The average θ_v through a layer above any nocturnal inversion but below the lid increases westward and in-

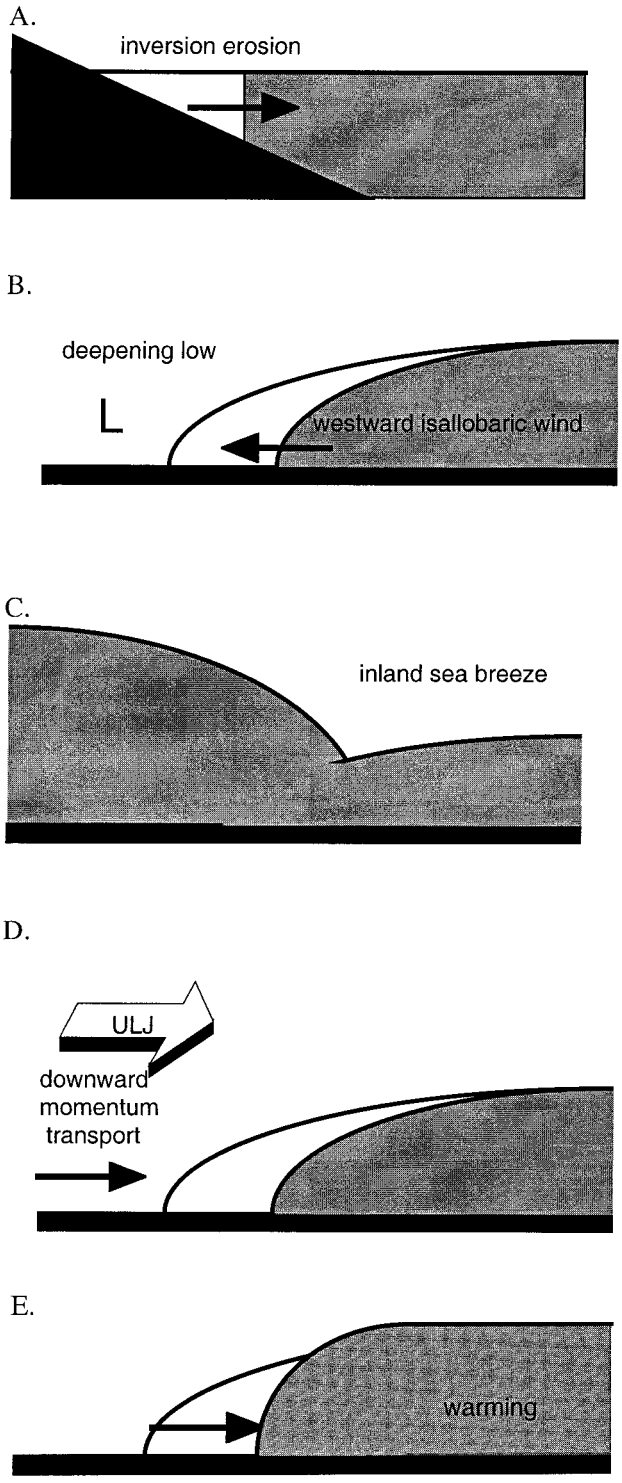

FIG. 2. Schematic diagrams of the (a) inversion erosion, (b) lee troughing, (c) inland sea breeze, (d) momentum mixing, and (e) static stability mechanisms.

creases from sunrise (1200 UTC) to sunset (0000 UTC). However the horizontal difference in θ_v was stronger at sunrise than at sunset.

The major dynamical feature of the dryline system below the lid is the low-level jet. The climatology of this southerly flow is documented by Bonner (1968) and Mitchell et al. (1995). Typically the jet speed is about 10–25 m s^{-1} but undergoes a strong diurnal variation. The jet is stronger at night. Hoecker (1963) details case studies where the jet speed is subgeostrophic during the day but reaches about twice its geostrophic value at night. The jet often displays multiple cores (Hoecker 1963; Djuric and Damiani 1980). Above the lid the winds are usually westerly. Ziegler and Hane (1993) note that the presence of secondary nonhydrostatic circulations near the leading edge of the line may help to form and maintain the dry front structure there.

The dryline undergoes a significant lateral movement during the day. Fujita (1958) and Beebe (1958) observed an eastward displacement of the dryline at about 5 m s^{-1}. Schaefer (1973) notes this daytime advance is greater before noon but the nighttime retreat is greatest before midnight. Lateral displacements of several hundred kilometers are often observed. Because convection is tied to the dryline, its location and movement is an important consideration in forecasting severe weather. Parsons et al. (1991) argue that the 21 April 1985 dryline behaved like a density current in the late afternoon as it started its nocturnal retreat. Wakimoto et al. (1996) observed a dryline with a density current structure using the ELDORA radar during VORTEX 95. Atkins et al. (1998) also argued that the dryline may propagate approximately like a density current. However, Crawford and Bluestein (1997) note that ''many drylines do not fit nicely into the current conceptual models'' of density current theory.

The earliest theories of the dryline system focused on its low-level jet component. Blackadar (1957) explained the diurnal variation of the jet as an inertial oscillation generated by the frictional decoupling of the boundary layer at night. During the day, the strong vertical transport of momentum by buoyantly driven convection leads to subgeostrophic flow. Around sunset the buoyantly driven convection ceases, a shallow nocturnal stable layer forms, decoupling the upper air from the effects of surface friction, and the subgeostrophic jet undergoes an inertial oscillation as it adjusts toward a geostrophic balance. Wexler (1961) advanced a theory of the climatological mean southerly jet. He applied the inertial boundary layer theories of the Gulf Stream to explain the jet as an intensification of the trade winds that are deflected poleward by the Rocky Mountains. The model assumes an inviscid reduced-gravity shallow-water semigeostrophic fluid on the beta plane. Wexler noted that the Blackadar mechanism could be incorporated into the model but did not do so. The present study merges the two theories.

Holton (1967) argued that the boundary layer diurnal

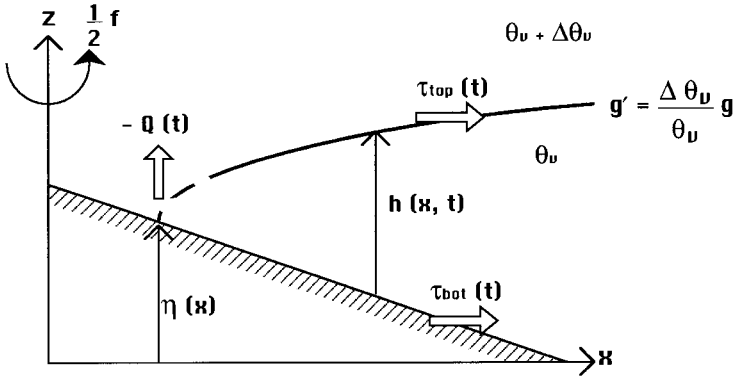

FIG. 3. Schematic diagram of the rotating, one-dimensional shallow-water model on an f plane. Rotation is indicated by the arrow around the z axis. The height of the inversion surface is h, and η is the height of the terrain. The virtual potential temperature difference between the two air masses denotes the stability or strength of the capping inversion (g'). The stress on the top layer is indicated by the arrow labeled τ_{top}. The stress on the bottom layer is indicated by the arrow labeled τ_{bot}. The dashed line represents mixing, and Q is the entrainment rate.

oscillation driven by differential heating due to the sloping topography is the major cause of the low-level jet. The literature (e.g., Bonner and Paegle 1970; Paegle and Rasch 1973; McNider and Pielke 1981; Parish et al. 1988; Fast and McCorcle 1990) supports the notion that the diurnally varying, terrain-induced pressure gradient above the nocturnal inversion enhances the flow's response to the frictional decoupling. Thus the theories of Holton (1967) and Blackadar (1957) are complementary. Neither theory, however, has been applied theoretically to the movement and structure of the dryline system.

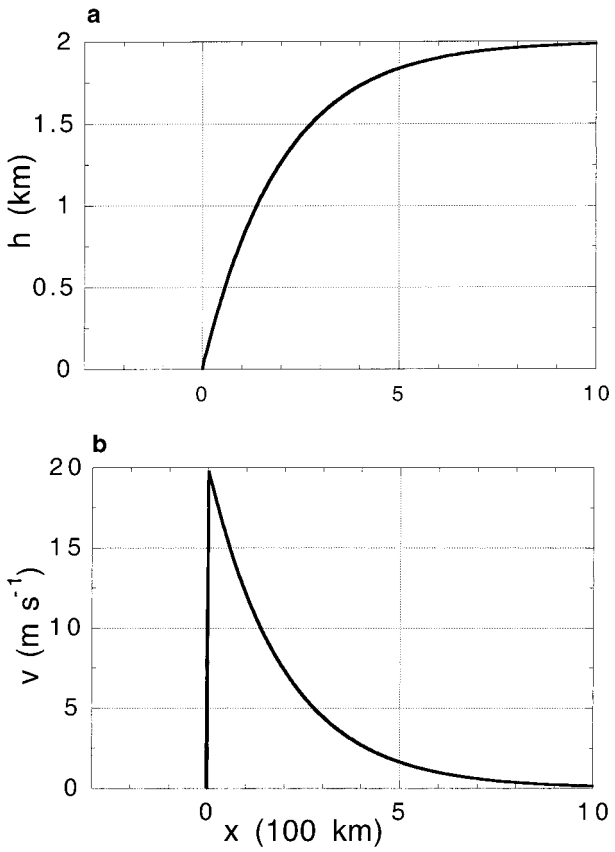

FIG. 4. Initial conditions of the shallow-water model represented in a cross section where (a) shows the height of the dry front or lid vs x, and (b) the meridional wind vs x.

There are several theories advanced to explain the diurnal variation of the movement of the dryline. It is first noted that the observed daytime-downslope and nighttime-upslope movement of the dryline is the opposite of that predicted by the theory of the mountain breeze (e.g., Defant 1951).

The first explanation of the eastward advance of the dryline was due to Schaefer (1973, 1974a,b). At dawn the inversion is essentially flat. Because of the sloping topography, the depth of the moist air increases from the dryline eastward. As the sun rises the surface is heated uniformly but the moist air is warmed more strongly closer to the dryline because its depth is smaller there. The inversion is readily broken adjacent to the dryline as the air aloft is entrained into the moist air so rapidly that its loses it maritime character. The dryline moves rapidly eastward but with diminishing speed because the erosion of the inversion is harder to achieve as the remaining moist air is deeper to the east. Figure 2a presents a schematic depiction of the inversion erosion process. The relatively flat lid has been transformed into a vertical airmass boundary at the dryline with a horizontal lid to the east. Note that there is no movement of air because the shallow wedge of moist air is eliminated by strong vertical mixing with the overlying dry air. Observational support for this idea is contained in Schaefer (1973) where he notes that the eastward movement of the dryline is not well correlated with the surface winds at the dryline. Ziegler

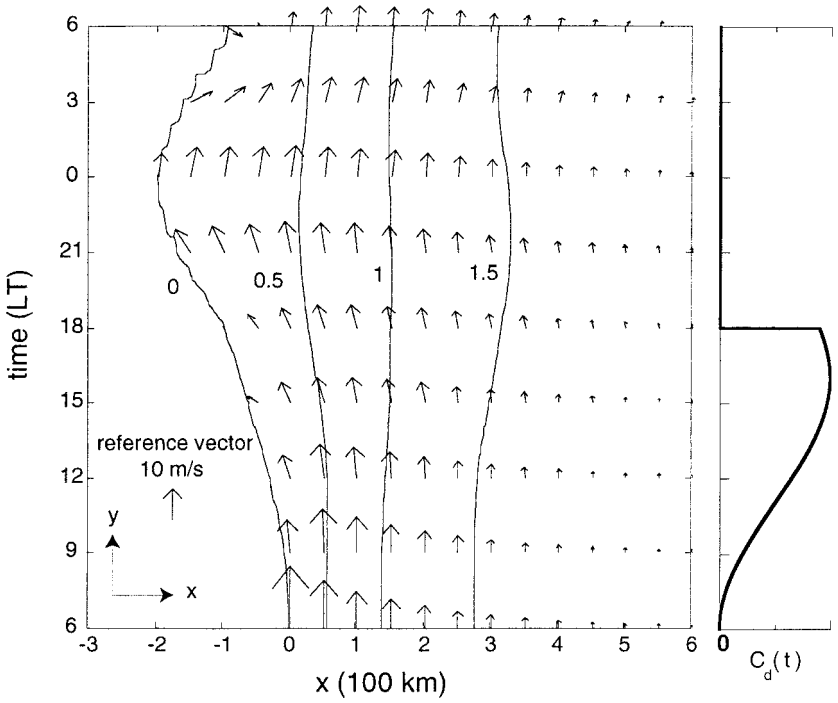

FIG. 5. Contour plot of the height (km) of the model inversion in x–t space for the case with only a diurnal variation in friction. The contour interval is 0.5 km. The wind vectors indicate both u and v components of the wind in x–y space. Wind speed is indicated by length. The temporal variation of the drag coefficient is given by the line plot on the right side of the figure.

and Rasmussen (1998) document a case (6 May 1995) when the mixing is unsteady and produces a discontinuous eastward movement of the dryline during the day. The steep daytime frontal surface of Fig. 2a is consistent with the observations of Fujita (1958), McGuire (1962), Ziegler and Hane (1993), and Ziegler and Rasmussen (1998).

The process of inversion erosion is irreversible and can only move the dryline downslope during the day. A different mechanism is needed to move the dryline back upslope. Benjamin and Carlson (1986) suggest that the diurnal variation in the lee trough located at or to the west of the dryline plays a role in this mechanism. The trough undergoes a daytime strengthening and a nighttime weakening associated with the insolation. There will be a westward isallobaric wind associated with the deepening low pressure to the west of the dryline that advects the dryline back upslope. Figure 2b presents a schematic diagram of this lee troughing. Bluestein et al. (1988) describe a tornadic storm near a dryline whose motion is consistent with this hypothesis. However, the origin of the observed deepening low is not unique. For example, it may be associated with an approaching synoptic disturbance from the west.

Another theory is that of Sun and Ogura (1979), who argue that surface differences across the dryline will lead to differential heating and an inland sea breeze. Their numerical simulation, however, does not reveal a dryline but rather a single mixed layer that is deeper on the warm side and shallower on the cool side. Figure 2c depicts a schematic of the inland sea-breeze model. The model is unrealistic for a west to east geometry (cf. Fig. 1). If applied to a north–south geometry, it is a possible model of a dryline curving eastward around its northern terminus. The study does emphasize the possible importance of differential surface heating due to variations in soil moisture, surface albedo, clouds, etc. McNider and Kopp (1990) show that cloud shading can sometimes be a major player in enhancing the baroclinic zone of the dryline.

McCarthy and Koch (1982) suggest an alternative mechanism for the eastward advance of the dryline. They emphasize the importance of vertical momentum mixing in the dry air to the west of the line. Typically there is southwesterly flow aloft in the dry continental air. During the day dry convection will mix the momentum down to the surface. The stronger surface westerlies that result from this transport will move the dryline eastward. This process may explain dryline bulges (i.e., localized greater eastward advancement of the dryline). Figure 2d presents a schematic of the momentum mixing mechanism. Numerical simulations of Sun and Wu (1992) and of Ziegler et al. (1995, henceforth ZMPW) support this theory. However, the latter simulation of 15-h duration only considers the daytime ad-

vance of the dryline and the beginning of the evening retrogression. The simulated dry front has a moisture structure similar to that observed (Ziegler and Hane 1993, henceforth ZH) (cf. Fig. 12a of ZH and Fig. 6a of ZMPW) but its lid structure is much shallower than the one observed (cf. Fig. 9d of ZH and Fig. 5b of ZMPW). The former simulation produces the complete diurnal simulation well but the imposed vertical shear of the zonal wind is needed to intensify the thermal and moisture gradients. Observationally the dryline frontogenesis is driven by a confluence zone of horizontal deformation. [Bannon (1983) has demonstrated for a quasigeostrophic fluid that a horizontal deformation field produces frontogenesis over a sloping topography.] Because of the sophisticated nature of the models used, it is not clear what the role of vertical momentum mixing is relative to, say, the diurnal variation of the surface friction.

Most recently Kovacs (1996) and Kovacs and Bannon (1997) have examined the diurnal variation of the dryline using a modified frontal model of Davies (1984). This model treats the cool moist air as an inviscid shallow-water fluid on an f-plane. A reduced gravity, g', reflects the stable stratification of the lid/dry front. The along-front wind is assumed to be in geostrophic balance. This semigeostrophic assumption and the assumption of uniform potential vorticity enable analytic solutions. The novel feature of the model is the use of a time-dependent reduced gravity. During the day the moist air is warmed and the strength of the lid is reduced. This behavior implies a diurnal variation of g' such that it is greater during the night and less during the day. With a prescribed $g'(t)$ undergoing a periodic variation, the Rossby radius of deformation $R = (g'h/f^2)^{1/2}$ also oscillates. The model predicts a dry front that is strong (i.e., has a large density difference) but shallow during the night and weak but steep during the day. This behavior is consistent with Margules frontal slope relation (Hess 1959). Figure 2e depicts a schematic of the static stability mechanism. In addition the model low-level jet is weak during the day and strong at night. Last the model dryline moves eastward during the day and retrogrades westward during the night. This behavior is a result of the geostrophic adjustment of the dry front as it maintains the strength of the along-front wind to be in balance with the horizontal pressure gradient. Most importantly the model vertical motion field exhibits convergence and rising motion to the east of the dryline near the end of the warming cycle. This feature is consistent with the typical dryline behavior of convective activity in the late afternoon.

The preceding review summarizes the current knowledge regarding the details of the dynamics of the diurnal variation in structure and location of the dryline. The literature suggests that a number of processes may be significant: sloping terrain, differential heating, diurnal variation in surface friction, Coriolis deflection, and diurnal variation in momentum mixing between the boundary layer and the free air aloft. Here we develop a shallow-water model to understand these processes in relation to the dynamics of the dryline system. This model will improve upon that of Kovacs and Bannon (1997) by including the effects of friction and by dropping the assumption of semigeostrophy.

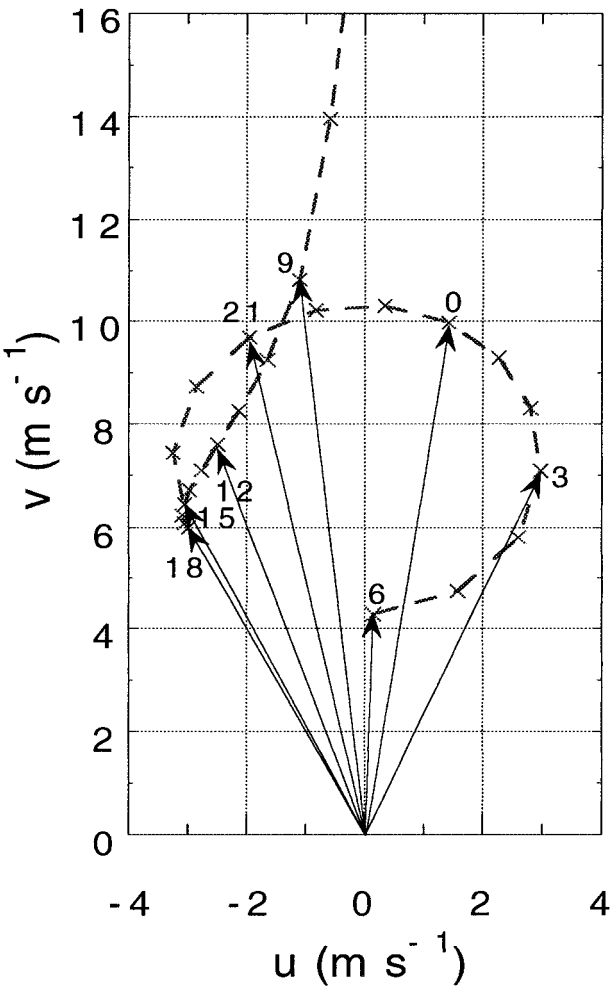

FIG. 6. Hodograph at $x = 2.5$ km for the case with only a diurnally varying friction. Wind vectors labeled in local time every 3 h. Winds greater than 12 m s^{-1} are associated with the initially large meridional wind and its subsequent deceleration with the inclusion of friction.

3. The model

The essential physics of the dryline system is contained in a rotating, shallow-water fluid on an f plane. Figure 3 illustrates the geometry and physics of the model dryline system. The x axis is normal and the y axis is parallel to the dryline. Henceforth we refer to these as the eastward and northward directions, respectively. The z axis is in the vertical. The u and v winds are parallel to the x and y axes, respectively. The dryline model is assumed to be one-dimensional with variations only in the x direction.

The fluid depth is denoted by h and the variable terrain height by η. The height of the free surface is $h + \eta$; $H = 2$ km is the maximum depth of the fluid far to the east. The terrain is either flat, $\eta = 0$, or is given by an exponential that decays to the east with an e-folding distance of 450 km. These choices for η enable analytic initial conditions (see section 3c).

a. Shallow-water equations

The model equations are

$$\frac{D\mathbf{u}}{Dt} + f\hat{\mathbf{z}} \times \mathbf{u} = -g'\nabla(\eta + h) + \left(\frac{\boldsymbol{\tau}_{\text{top}} - \boldsymbol{\tau}_{\text{bot}}}{\rho_0 h}\right), \quad (1)$$

$$\frac{\partial h}{\partial t} + \nabla \cdot (h\mathbf{u}) = Q, \quad (2)$$

where $D/Dt = \partial/\partial t + u\partial/\partial x$, $\mathbf{u} = (u, v)$ = the horizontal velocity, $f = 1 \times 10^{-4}$ s^{-1} is the Coriolis parameter, g' is a reduced gravity, $\boldsymbol{\tau}_{\text{top}}$ is the stress on the top layer, $\boldsymbol{\tau}_{\text{bot}}$ is the stress on the bottom layer, ρ_0 is a constant reference density, and Q is a mass source term. A reduced gravity g' models the stable stratification of the dry front

$$g' = g\frac{\Delta\theta_v}{\theta_v}, \quad (3)$$

where $g = 10$ m s^{-2} is gravity, $\Delta\theta_v$ is the virtual potential temperature between the two air masses, and θ_v is the virtual potential temperature of the shallow dense fluid. The diurnal variation in the static stability (Kovacs 1996) is modeled with a prescribed temporal variation in the reduced gravity.

The quadratic form of surface friction (e.g., Stull 1988, section 7.4) is used:

$$\tau_{\text{bot}} = \rho_0 C_d |\mathbf{u}| \mathbf{u}, \quad (4)$$

where C_d is the dimensionless drag coefficient. Though C_d depends on the surface roughness and the atmospheric stability near the surface, it is taken to be spatially uniform in our experiments. In order to model the diurnal variation in surface friction (e.g., Blackadar 1957), the drag coefficient undergoes a prescribed temporal variation.

The stress on the top layer, τ_{top}, represents the addition of momentum as air aloft is entrained across the dry front (e.g., Stull 1988, section 7.4). This process is expressed by the equation

$$\tau_{\text{top}} = \rho_0 Q(\mathbf{u}_{\text{top}} - \mathbf{u}), \quad (5)$$

where $Q > 0$ is the prescribed entrainment of warm dry air across the dry front during the day and $\mathbf{u}_{\text{top}}$ is the prescribed horizontal velocity of the air aloft. Because the model only describes the dynamics of the cool moist air, the process of momentum mixing can only be incorporated on the east side of the dry front. Thus our test of the theory of McCarthy and Koch (1982) is only a partial one.

The process of inversion erosion (Schaefer 1973) may be modeled using the mass source term Q. Entrainment, or a mixing of the air masses, will occur across the dry front capping inversion. Because the amount of solar heating of the boundary layer needed to break the inversion is dependent on the depth of the fluid (h), the shallowest areas of fluid will most likely be eroded first. Because the dry front is shallowest at its western edge, the inversion erosion will typically be greatest there. Thus we specify a mass sink ($Q < 0$) only at the dryline in order to model this process of inversion erosion.

The momentum equation (1) does not assume a geostrophic balance. Indeed Ziegler and Hane (1993) estimated from observations that the inertial accelerations are as significant as the Coriolis term. [They further estimated that the hydrostatic approximation, upon which the shallow-water equations are based, is valid everywhere except in a narrow (~8 km) transition region across the dryline.] Thus the model dryline will have the freedom to behave as a flow in geostrophic balance as Wexler (1961) and Kovacs (1996) assumed or to take on the attributes of a density current as the observations of Parsons et al. (1991) suggest. In the absence of friction, topography, and a mass source, the shallow-water set (1) and (2) can describe many aspects of such nonlinear phenomenon as gravity currents, hydraulic jumps, and bores (e.g., Kuo and Polvani 1997). Its major limitation is the hydrostatic assumption. The appendix reviews the solution to the dam-break problem, a relevant description of the model results simulating the westward surge of the dryline in the late afternoon.

This model combines the theories of Wexler (1961), Blackadar (1957), McCarthy and Koch (1982), and Kovacs (1996) in a format that will allow the model dryline to exhibit balanced flow, inertial oscillation, and gravity current behavior. The model also permits the generation of pressure jumps as proposed by Tepper (1955). Section 4 presents a series of controlled numerical experiments that assess the important physical processes of each theory, individually and in combination.

b. Numerical techniques

The governing equations are solved using finite differencing with the momentum- and mass-conservative flux form as described in Schär and Smolarkiewicz (1996). Their algorithm makes it possible to handle the case where the depth of the dry front goes to zero. The rotational and frictional terms are coded using classical implicit numerics, specifically a trapezoidal finite-differencing scheme. The pressure gradient term follows the work of Smolarkiewicz and Margolin (1993). The model uses a staggered grid, having h and v together on the horizontal step, and u a half step off. The grid

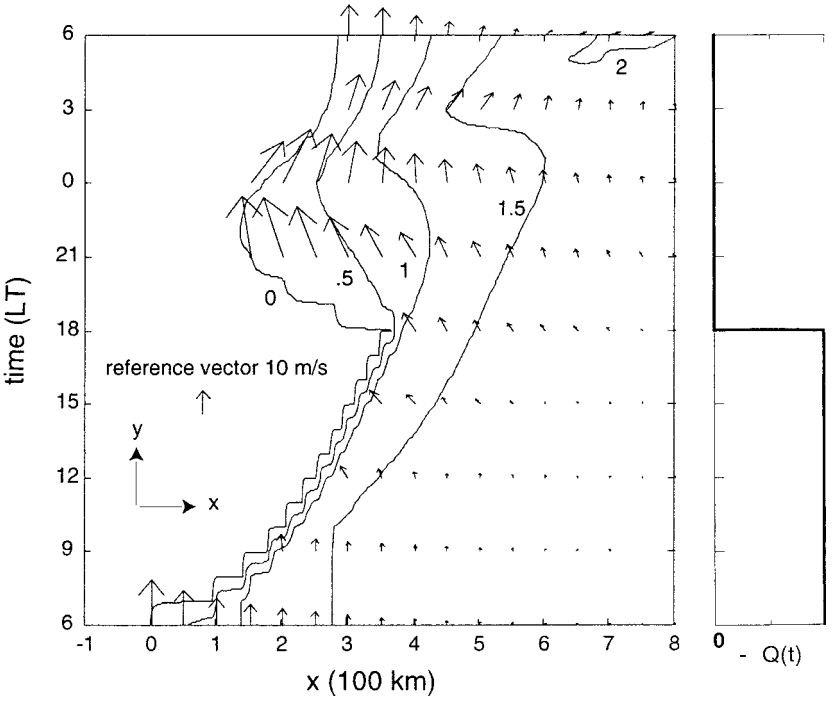

FIG. 7. Model fields for the case with only a diurnally varying entrainment. Height contours and velocity vectors as in Fig. 5. The temporal variation of the inversion erosion at the dryline is given by the line plot on the right side of the figure.

spacing is 2.5 km. The model domain is 2×10^3 km. The time step is 45 s.

Several tests were conducted to verify the model numerics. The model successfully simulates the spreading out of a nonrotating shallow-water drop (Schär and Smolarkiewicz 1996). With rotation the model matches the period of oscillation solved by Frei (1993). When the model is initialized with the analytic initial conditions for the model dryline (see section 3c) the model dryline without friction or a mass source remains stationary. Last the appendix demonstrates the model's ability to simulate the dam-break problem. The numerical solution is compared to the analytic solution to the nonrotating case. The model is then used to assess the effect of rotation.

c. Initial and boundary conditions

The initial conditions of the model are an f-plane version of the Wexler model of the climatological mean southerly jet in geostrophic balance. The shallow-water equations have an exact nonlinear, uniform potential vorticity, steady-state solution without friction ($\boldsymbol{\tau} = 0$) and a mass sink ($Q = 0$). The no-terrain form of the exact nonlinear solution is, valid for $x > 0$,

$$u = 0, \qquad v = \sqrt{g'H}\,\exp(-x/R), \tag{6}$$

$$h = H[1 - \exp(-x/R)], \tag{7}$$

where

$$R = \frac{\sqrt{g'H}}{f} \tag{8}$$

is the Rossby radius of deformation. Unlike in Wexler (1961) there is no need for a rigid wall at $x = 0$. Kovacs (1996) provides the solution with an exponential topography similar to that of the Great Plains.

The no-terrain initial conditions for h and v (Fig. 4) exhibit a low-level jet with a maximum of 20 m s^{-1} at the western edge of the dryline system where $h = 0$. There is no initial u velocity. The maximum height of the dry front is 2 km. These conditions are assumed to reflect a mean dryline system valid at dawn (0600 LT). The v field decays exponentially with distance from the dryline, the fluid depth increases exponentially. The e-folding scale is the Rossby radius of deformation. For the reference settings $H = 2$ km, $f = 1 \times 10^{-4}$ s^{-1}, and $g' = 0.2$ m s^{-2} the Rossby radius is $R = 200$ km.

The eastern boundary in the x direction is open such that the normal gradient of each variable is set to zero. Test results proved that this condition is acceptable, because there is little reflection at the boundary. The western edge of the fluid where h vanishes is treated following Schär and Smolarkiewicz (1996). This scheme uses an upstream differencing of the advective terms in flux form, which keeps the fluid depth h nonnegative, with a flux correction to reverse the effects of the computational diffusion. Momentum averaging, rather than velocity averaging (Schär and Smith 1993) is used to

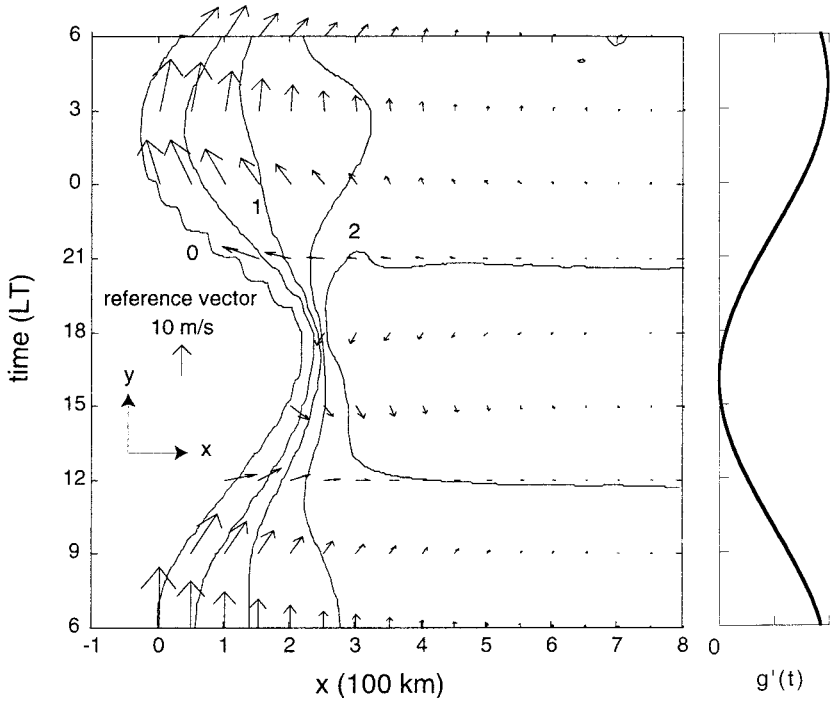

FIG. 8. Model fields for the case with only a diurnally varying stability. Height contours and velocity vectors as in Fig. 5. The temporal variation of the static stability is given by the line plot on the right side of the figure.

keep the velocity fields bounded in regions where the depth of the fluid is vanishing. Tests of the algorithm (Schär and Smolarkiewicz 1996; Miller 1998) indicate that the scheme can accurately handle both advancing and retreating layers of fluid.

4. Effects of individual physical processes

In this section we test the effect of diurnal variation in the surface friction, stability, inversion erosion, and momentum mixing individually. In the first three experiments the model is initialized with the analytic solution (6) and (7) for the no terrain case. In the fourth experiment the model includes terrain and the initial height of the dry front is uniform in order to maximize the effect of the momentum mixing. In each experiment the initial model time $t = 0$ corresponds to 0600 LT. The results of 1-day simulations are presented. All wind velocities discussed in this section are the maximums found over the whole domain for the time indicated. The dryline movement is measured using the zero fluid depth contour ($h = 0$).

a. Diurnal variation of friction

The daily cycle of surface friction is incorporated into the shallow-water model by using a time-dependent drag coefficient, C_d, of the form

$$C_d(t) = \begin{cases} 2 \times 10^{-3}\left[1 - \cos\dfrac{\pi t}{10h}\right] & \text{from 0600 to 1800 LT} \\ 0 & \text{otherwise.} \end{cases} \quad (9)$$

This choice yields a surface friction that increases from zero at sunrise (0600 LT; $t = 0$) to a late afternoon maximum at 1600 LT, and then instantly drops to zero at sunset (1800 LT) as in Blackadar (1957).

Figure 5 presents the results for the case with only a diurnal variation in friction. The drag coefficient C_d is given by (9), the reduced gravity g' has the constant value of 0.2 m s^{-2}, and the mass source term Q is set to zero. The right panel plots the drag coefficient as a function of time along the ordinate. The left panel is a contour plot of the height of the dry front in x–t space. The velocity vectors denote the wind field in x–y space. Similar figures are presented for other experiments.

Initially the wind field is southerly and in geostrophic balance. With the onset of surface friction, the velocity becomes subgeostrophic and there is cross-isobaric flow to the west. During the day, the meridional wind decreases rapidly from 20 to 7 m s^{-1} due to the increasing friction. The zonal winds become westward during the day due to cross-isobaric flow toward lower pressure. At sunset, the frictional drag has ceased and the merid-

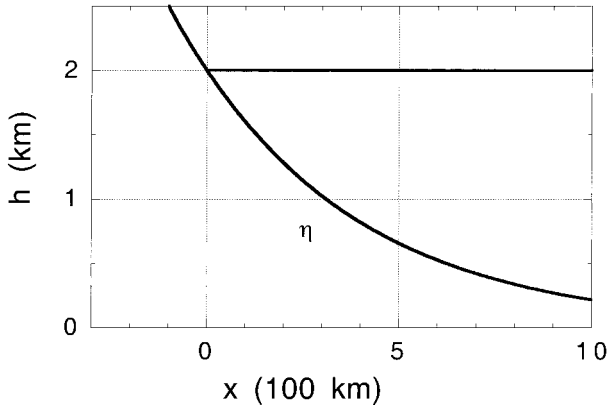

FIG. 9. Initial conditions of the shallow-water model for the case with only a diurnal variation in momentum mixing. Cross section of the height of the dry front or lid vs *x*.

ional wind increases rapidly to 10 m s^{-1} northward. Coriolis deflection of these strong southerly winds creates westerly velocities by midnight. An inertial oscillation (Fig. 6), as described by Blackadar (1957), is observed due to the removal of friction at sunset. The maximum v velocity occurs near midnight (2245 LT), in accordance with the nocturnal low-level jet theory of Blackadar (1957).

In response to these winds the dryline moves slightly westward during the day (about 100 km) and the slope of the dry front (indicated by the zonal gradient of the *h* field) is reduced. By midnight the dryline is about 200 km to the west of its starting position. Due to the commencement of westerly winds by midnight, the dryline moves eastward 125 km from midnight until dawn. These changes in dry front structure and dryline position are contrary to observations.

b. Diurnal variation of inversion erosion

Insolation will drive rapid entrainment of dry air across the dry front where it is shallowest. This process is represented in the model as a mass sink, *Q*, in the continuity equation of the form

$$Q(t) = \begin{cases} -4.8 \text{ m s}^{-1} & \text{from 0600 to 1800 LT} \\ 0 & \text{otherwise.} \end{cases} \quad (10)$$

This mass sink is applied only at the western edge of the dry front. Numerically it is applied at the grid point with the shallowest fluid depth. The amplitude of the mass sink is chosen to produce a representative erosion of the inversion of about 3–400 km, consistent with observations and the model of Schaefer (1974a). For simplicity we take the temporal variation of the erosion to be constant during the daytime and to vanish during the nighttime. In reality its variation is a complex function of the depth of the layer; the strength of the daytime heating, which drives the mixing; and the nature of the vertical and lateral entrainment. Inclusion of such processes is outside the scope of this investigation.

Figure 7 presents results for this process of inversion erosion only. The mass source term *Q* is given by (10), the reduced gravity g' has the constant value of 0.2 m s^{-2}, and the drag coefficient C_d and the top stress (5) are set to zero. During the day, mass and momentum are removed causing an eastward progression of the dryline of over 300 km and the elimination of the low-level jet. The slope of the dry front is very steep (i.e., about 20:1) near the dryline. Despite the eastward movement of the dryline, the zonal wind is westward as the moist air flows toward the mass sink at the dryline ($h = 0$). This cross-isobaric flow is not due to friction, which is absent in this experiment, but due to the mass sink in (2). The sink produces falling pressure and cross-isobaric isallobaric flow. After the initial decrease in the meridional wind, the southerly wind increases due to the Coriolis deflection of the westward wind.

The ''stair-step'' nature of the dryline displayed in Fig. 7 and elsewhere is a consequence of the steep slope of the dry front when a mass sink is present and of the fact that the fields are sampled at 1-h intervals. No smoothing has been performed to the fields.

At sunset (1800 LT) the erosion ceases and the dryline surges westward, moving 250 km in 3 h. This surge is analogous to the gravity current behavior of the dryline described by Parsons et al. (1991). The surge is followed by a 150-km return to the east as the winds undergo an anticyclonic Coriolis defection. The height field spikes to 2.4 km just before sunrise near $x = 700$ km, about 400 km to the east of the dryline. This feature constitutes a 0.8-mb pressure rise with eastward winds of 5 m s^{-1}, and is similar to (though weaker in magnitude than) the pressure jump of Tepper (1955). The zonal wind becomes eastward at midnight corresponding to the eastward movement of the dry front. A sharp increase in the meridional wind is observed by 2100 LT, but the wind decreases until dawn due to the Coriolis deflection of the strong eastward flow. The maximum southerly wind of over 30 m s^{-1} occurs at 2100 LT near the dryline. Farther to the east the winds are strong around midnight and decrease toward dawn, a behavior similar to the nocturnal low-level jet, described by Bonner (1968).

The behavior of the model in this case differs sharply from the analytic model of inversion erosion in Kovacs (1996) that uses a semigeostrophic assumption. In that study the slope of the dry front is constant as the dryline progresses eastward during the day and there is no retrogression at night.

In addition to the erosion process at the western edge of the line, there is also entrainment of air across the inversion. To incorporate this process into the model we added to (10) a representative uniform mass source of 2 cm s^{-1} (Stull 1988, section 11.4.5) everywhere along the dry front from 0600 to 1800 LT. Again the top and bottom stresses are set to zero. The results (not shown)

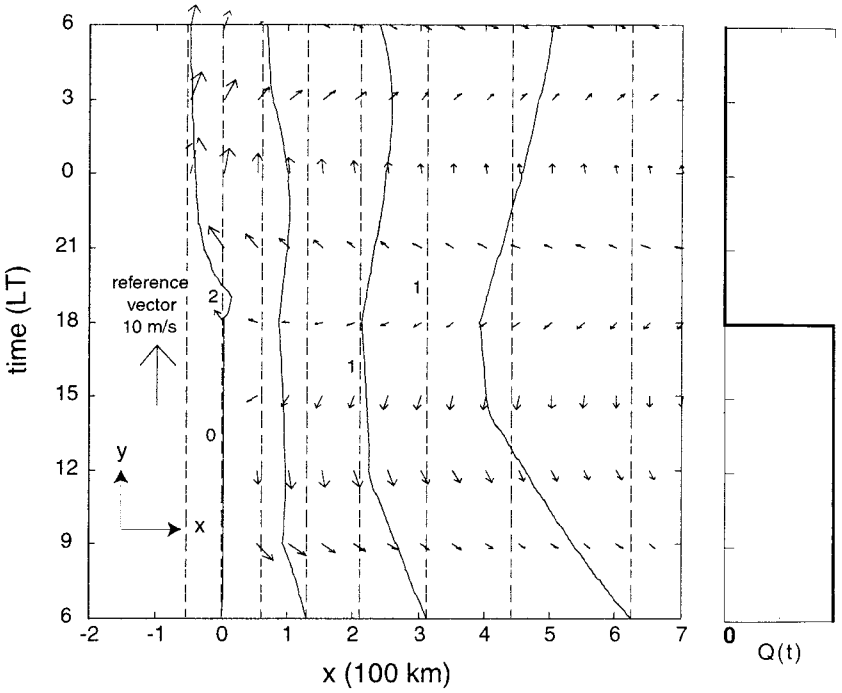

FIG. 10. Model fields for the case of a diurnally varying momentum mixing. Dashed lines indicate the height of the terrain with contour interval of 0.25 km. Height contours and velocity vectors as in Fig. 5. The temporal variation of the entrainment across the dry front is given by the line plot on the right side of the figure.

are similar to those displayed in Fig. 7. The major difference is that the addition of mass confined the eastward advance of the dryline to the late morning hours and reduced its amplitude from 350 to 200 km.

c. Diurnal variation of stability

The combination of short- and longwave radiative processes tends to reduce the static stability during the day and increase it during the night. This process is represented in the model by a prescribed diurnal variation of the reduced gravity of the form

$$g'(t) = 0.1 \text{ m s}^{-2} \frac{\left[1 + \cos\left(\pi \frac{t + 2h}{12h}\right)\right]}{(1 + \cos\pi/6)}. \quad (11)$$

The reduced gravity is largest before sunrise (0400 LT; $t = -2h$) and vanishes in the afternoon (1600 LT). At $t = 0$ the reduced gravity has the value used in the initial conditions and that used in the other model runs. We recognize that observations indicate that the strength of the inversion does not completely vanish during the afternoon to the east of the dryline. We allow the model reduced gravity to vanish here in order to maximize the impact of the variation in the static stability. Model runs (not shown) with a smaller variation in g' (such that g' remains positive) show qualitatively similar results as those displayed here.

Figure 8 presents results with only the diurnal variation in static stability. The reduced gravity g' is given by (11), and the mass source term Q and the drag coefficient C_d are set to zero. The reduction in stability during the day moves the dryline eastward until 2100 LT and the slope of the dry front steepens. The eastward progression of 200 km is associated with eastward zonal winds and first a reduction in the southerlies and then their elimination and replacement with northerlies. Physically the reduction in the reduced gravity decreases the zonal pressure gradient and the flow becomes supergeostrophic and is deflected to the right. This process causes the zonal westerlies, the steepening of the dry front, and the movement of the dryline. In the model the geostrophic southerly winds are driven by the pressure gradient force associated with the horizontal variation of the inversion height. Because this force is proportional to the reduced gravity, as g' tends to zero the geostrophic southerlies must disappear.

After 2100 LT the increasing static stability moves the dryline westward 300 km and the slope of the dry front flattens considerably. During this period the zonal wind is easterly while the meridional wind increases during the night with a maximum near midnight. The

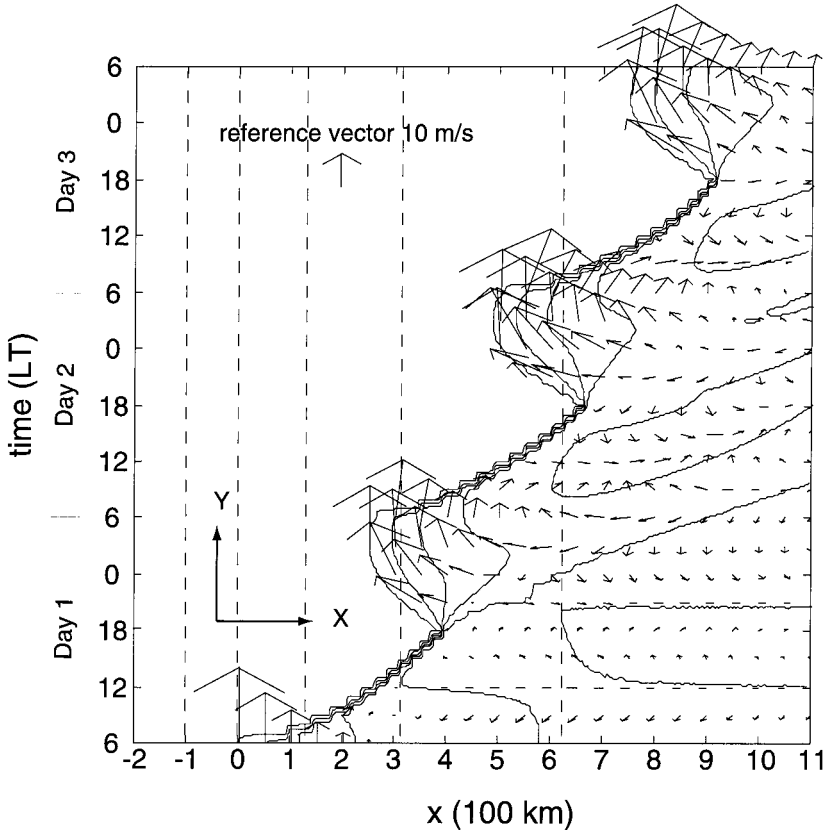

FIG. 11. Model fields for the case of a diurnally varying friction, entrainment, and stability plus terrain. Terrain contours as in Fig. 10. Height contours and velocity vectors as in Fig. 5.

maximum meridional wind of 17.6 m s^{-1} occurs about 9–12 h after the minimum in the reduced gravity. For the choice (11) this timing coincides with the nocturnal low-level jet of Bonner (1968).

Model simulations with topography are similar to that displayed in Fig. 8 but with a weaker amplitude. The inclusion of topography allows a diurnal variation to be driven by the pressure gradient term $-g'\nabla\eta$ in the momentum equation (1). For topography decreasing to the east this term drives westward (upslope) motion during the day and eastward (downslope) motion at night. This behavior is opposite to the variation exhibited in Fig. 8 and explains the weaker variation when topography is included.

d. Diurnal variation of momentum mixing

The entrainment of air from aloft into the moist air below the dry front also produces a transport of the upper-air momentum into the moist air. This transport of momentum downward is represented in the model by a stress on the top of the inversion, expressed by (e.g., Stull 1988)

$$\boldsymbol{\tau}_{\text{top}} = \rho_0 Q(\mathbf{u}_{\text{top}} - \mathbf{u}), \tag{12}$$

where the wind aloft, $\mathbf{u}_{\text{top}}$, is taken to be zonal with the representative amplitude of 10 m s^{-1}; ρ_0 is the constant reference density; and the entrainment rate $Q = 2$ cm s^{-1} (e.g., Stull 1988, section 11.4.5) during the day, but zero at night, to simulate the diurnal variation of mixing, which is driven primarily by surface heating. Here the entrainment rate, Q, is applied uniformly over the whole dry front.

We use slightly different initial conditions to agree with the work of Schaefer (1974a). The momentum mixing initial conditions (Fig. 9) are those of a resting shallow-water fluid with no initial **u** field and a uniform free-surface height of 2 km. Sloping terrain is included so that even though the height of the fluid is constant, the depth, h, changes. The equation for the depth of the fluid is

$$h = H(1 - e^{-x/b}), \tag{13}$$

where $H = 2$ km, and the e-folding distance $b = 450$ km. The use of this initial condition with terrain produces a very shallow layer of fluid near the dryline. Because the effect of momentum mixing (12) is enhanced over shallow terrain where the fluid depth, h, is

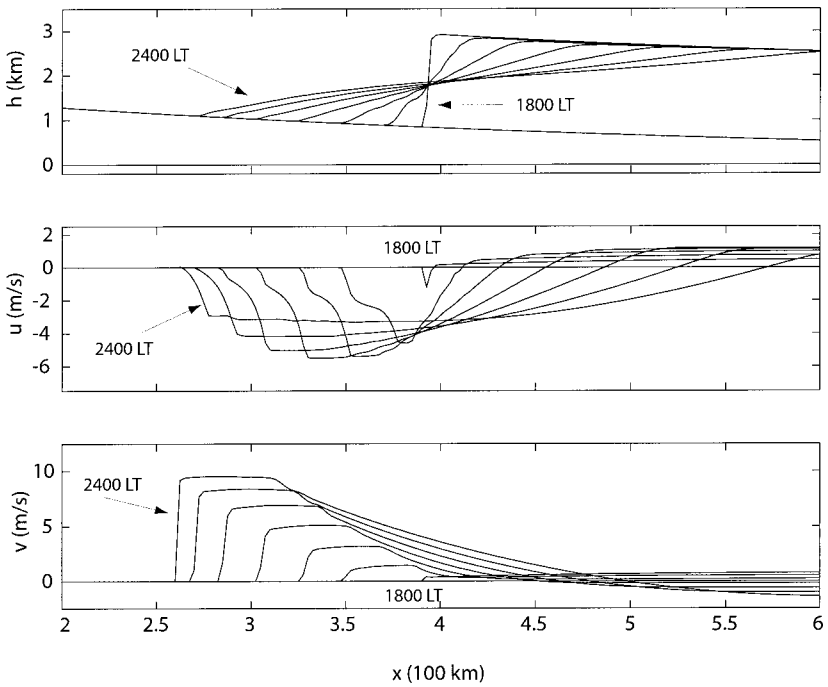

FIG. 12. The height field, h, the zonal wind, u, and the meridional wind, v, as a function of horizontal distance, x. The fields are plotted hourly from 1800 LT to 2400 LT for the westward surge of the dryline during the first day of the simulation depicted in Fig. 11.

small [see (1)], this choice will tend to maximize the effect of momentum mixing.

Figure 10 presents the results with only the process of momentum mixing. The mass source term Q is as specified above, the reduced gravity g' has the constant value of 0.2 m s^{-2}, and the drag coefficient C_d is set to zero. During the day, mass and westerly momentum are added over the domain of the dry front through mixing with air above the inversion. The height of the inversion increases due to this addition of mass. The addition of westerly momentum initially moves the dry front a little to the east. The westerly flow is greatest close to the dryline where the fluid is most shallow and decreases toward the east. This behavior reflects the fact, evident in (1), that the effect of the stress terms is enhanced where the fluid is shallowest. This convergent pattern tends to steepen the slope of the dry front. The eastward flow in the late morning changes to westward in the afternoon by the pressure gradient force acting to the west due to the pileup of mass to the east. The zonal wind turns weakly westward when the pressure gradient dominates in the afternoon. The meridional wind is initially southward due to Coriolis deflection of weak eastward flow, but turns northward by 1500 LT due to Coriolis deflection of weak westward velocities. After sunset (1800 LT), the addition of mass and momentum ceases. The dryline moves westward and the slope of the dry front flattens. The westward zonal wind is deflected northward to produce strong southerly flow near midnight.

This experiment and others using different initial conditions (not shown) indicate that vertical momentum mixing has little effect on the model dryline.

5. A shallow-water model of the dryline system

A model run with all the physical processes considered in the preceding section (exception the diurnal variation in momentum mixing, which does not show significant effects) in the presence of terrain provides a simulation of the dryline system. The initial conditions (Kovacs 1996) are the uniform potential vorticity solution with topography (13). The results for 3 days are presented in Fig. 11. Note the repetition of the patterns in the height contours and wind vectors. This feature suggests that the 1-day model runs are not sensitive to the initial conditions. Each day the dryline propagates approximately 400 km eastward, and each night it retrogresses about 150 km westward. The slope of the dry front is small in the morning and overnight, but nearly vertical in the afternoon, in agreement with observations. Nocturnal jets are observed near and after midnight close to the dryline, in agreement with Bonner (1968). The dryline moved roughly 750 km in 3 days. This distance is reasonable and corresponds to the distance between

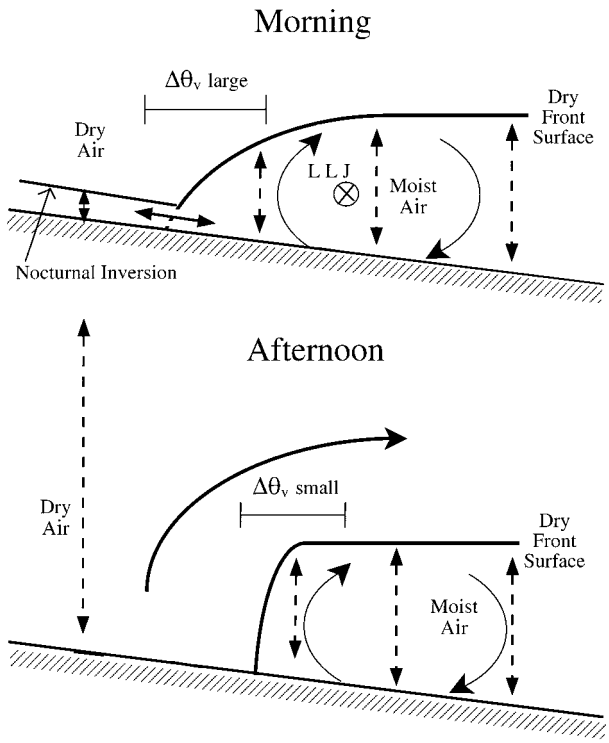

FIG. 13. Schematic cross section of the dry front in the morning (top) and afternoon (bottom). Solid lines indicate inversion surfaces. Hatching indicates the sloping terrain. Vertical dashed lines with arrows at both ends indicate vertical turbulent transport. Solid curves with single arrows indicate the sense of the secondary circulation below the inversion as well as flow aloft in the afternoon. Brackets indicate virtual potential difference between the two air masses. The position of the northward low-level jet (LLT) is indicated by the circled cross in the morning.

El Paso, Texas, to halfway across Texas, or from Midland, Texas, to the Texas–Louisiana border.

Figure 12 documents the nature of the westward surge of the dryline. At dusk (t = 1800 LT) the dry front is nearly vertical at the line with a slope of about 1:5 and flat to the east; the winds are weak. The dryline surges westward with wind speeds near 5 m s^{-1}. These westward winds are deflected by the Coriolis force to produce southerly flow. This southerly flow is a maximum in the early morning (0100–0300 LT). After midnight the dryline remains stationary and the slope of the dry front is about 1:100.

The motion of the dryline system in Fig. 12 is similar to that displayed in the appendix (Fig. A3) for the dam-break problem for a rotating fluid. There are important quantitative differences. The reduced gravity for the dryline is much less than for the dam-break simulation. This difference explains the weaker winds seen for the dryline case. In addition the dryline reduced gravity increases during the night; this behavior helps to stabilize the system in the early morning (t = 0000–0600 LT).

6. Conclusions

A shallow-water model has been utilized to test various theories of the diurnal variation of the dryline system. The case of a diurnal variation of surface friction produces a nocturnal low-level jet but fails to capture the eastward movement of the dryline and the steepening of the dry front during the day. The case of downward mixing of momentum from the flow aloft into the moist air fails to produce a significant effect on the model dryline. The case of inversion erosion produces an eastward movement and steepening of the dry front during the day. A southerly wind maximum is produced but relatively early in the evening. The case of diurnal variation in stability produces an eastward movement of the line during the day but the steepening of the dry front is limited to the late afternoon. At night a southerly wind maximum occurs near midnight but the nighttime westward retrogression is larger than the daytime progression. Thus no single physical process can capture all the salient features of the observed dryline system.

The case of a combination of friction, entrainment, stability, and terrain satisfies all of the observational criterion. The case produces a reasonable eastward progression during the day, a weaker westward retrogression during the night, and net eastward movement for 3 days. The slope of the inversion and the southerly wind agree with observations: the slope is steepest during the day and the southerly winds reach a maximum near midnight. It appears that a combination of processes results in a closer match to observations than the individual processes.

Figure 13 presents a conceptual model of the diurnal variation of the dry front system that synthesizes our results as well as other researchers. It extends the model of Fig. 1 to include a nocturnal inversion within the dry air (Schaefer 1974a,b; 1986; see also Kovacs 1996) as well as secondary circulations in the moist air (Ziegler et al. 1997). At dawn the dry front/lid caps the moist air and intersects, not the terrain, but a shallow (~100 m) nocturnal boundary layer that formed in the air overnight. Below this nocturnal boundary layer the temperature gradient may reverse itself to be eastward with colder temperatures in the dry air. Lateral surface mixing between the air masses may then occur causing the moisture gradient to weaken and the dryline would appear weak and ill defined. When the surface heating commences at sunrise, the turbulent vertical heat transport quickly erodes this nocturnal boundary layer and the surface moisture gradient moves rapidly eastward and intensifies. Because the vertical heat transport is confined by the dry front lid to the east of the dryline but is unconfined to its west, the moist air is warmed more than the dry air. This uneven warming decreases the density difference between the two air masses. As a consequence the dry front steepens and moves farther eastward. The surface heating during the day leads to

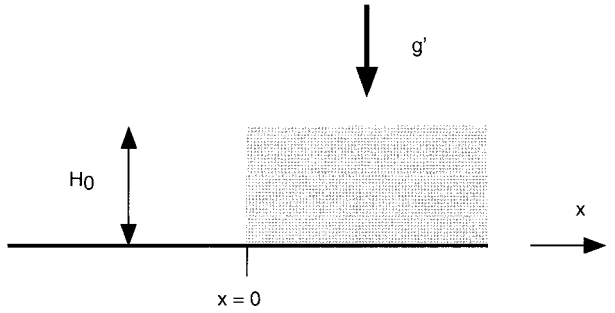

FIG. A1. Schematic illustration of the initial conditions for the dam-break problem.

strong vertical momentum transports and the nocturnal low-level jet formed overnight is destroyed by this surface friction. At dusk the surface heating and surface friction wane and the moist air undergoes an inertial oscillation and rapidly advances westward. This westward motion is enhanced with the establishment of a stronger density difference across the dry front as the moist air cools. The Coriolis deflection of this westward ageostrophic wind generates the nocturnal low-level jet in the moist air. Over the dry air a shallow nocturnal boundary layer forms overnight. The process then repeats itself at dawn the next day.

The present modeling effort is not without some limitations. One is that the amplitude and structure of the variations in surface drag, inversion erosion, entrainment and stability changes are prescribed. The evolution of these quantities could be predicted by transforming the present shallow-water model into a mixed layer model driven by prescribed surface fluxes of heat and moisture. A second is that the detailed structure of the nonhydrostatic behavior of the leading edge of the dryline with its secondary internal circulations cannot be captured in our shallow-water model.

Acknowledgments. We thank Christoph Schär for making his shallow-water numerical code available for our use in this study and Patrick A. Jones for programming assistance. Partial financial support was provided by the National Science Foundation (NSF) under NSF Grants ATM-9424462 and ATM-9729631.

APPENDIX

Numerical Solution of the Dam-Break Problem for a Rotating Fluid

The classic dam-break problem describes the evolution of a semi-infinite layer of fluid acting under the influence of gravity that is initially at rest with a uniform depth H_0. Figure A1 describes the geometry of the problem considered here. It is the idealization of the instantaneous removal of a vertical wall at $x = 0$ at the initial time $t = 0$. In the nonrotating case, the shallow-water solution in the absence of a mass source and friction is, in the present geometry (see, e.g., Acheson 1990),

$$\left.\begin{aligned} h(x,t) &= \frac{H_0}{9}\left(2 + \frac{x}{c_0 t}\right)^2 \\ u(x,t) &= -\frac{2c_0}{3}\left(1 - \frac{x}{c_0 t}\right) \end{aligned}\right\} \quad \text{for } -2c_0 t < x < c_0 t, \quad \text{(A1)}$$

where

$$c_0 = \sqrt{g' H_0}. \quad \text{(A2)}$$

Elsewhere the flow fields retain their initial values. Figure A2 compares the analytic solution to a model run with the parameter settings $g' = 0.20$ m s^{-2} and $H_0 = 2$ km, implying $c_0 = 20$ m s^{-1}. The horizontal and temporal resolution is the same as the other model runs in this paper. The comparison indicates that the numerical model does an excellent job in capturing the

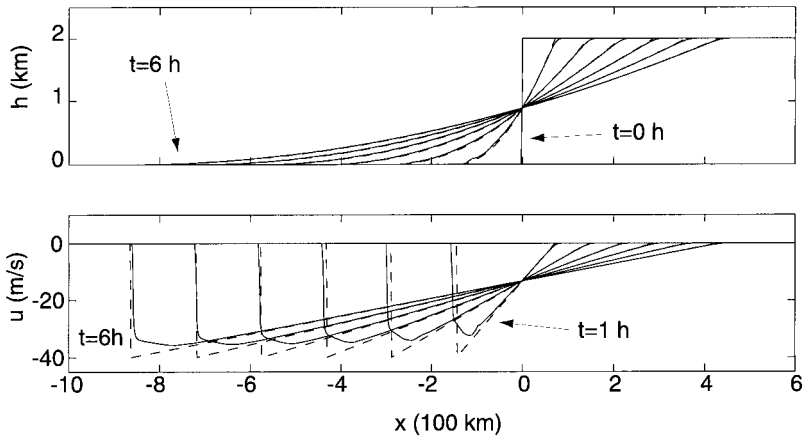

FIG. A2. Analytic (dashed) and numerical (solid) solution of the nonrotating dam-break problem. The solutions for the height field, h, and the zonal wind, *u*, are plotted at the times $t = 0$, 1, 2, 3, 4, 5, and 6 h. The meridional wind (not shown) is identically zero for all time.

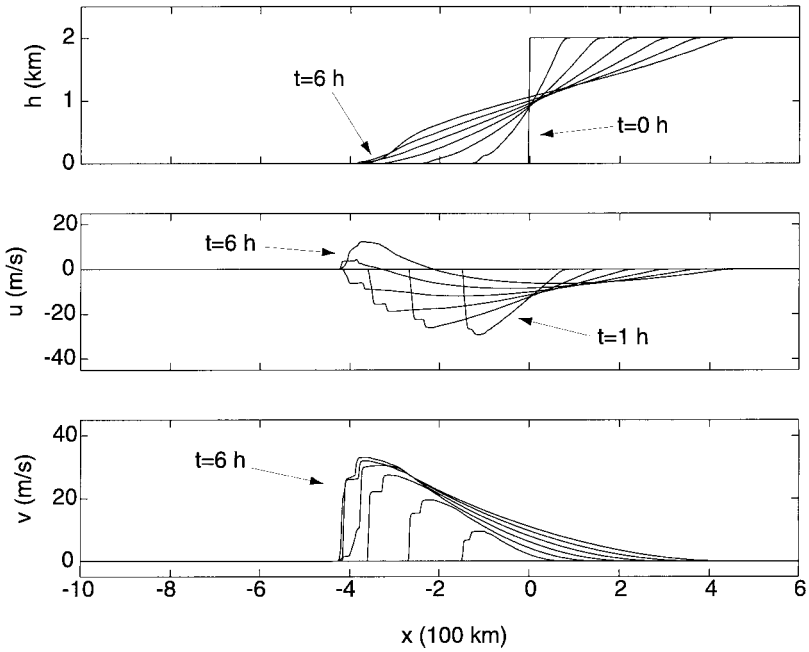

FIG. A3. Numerical solution of the dam-break problem of Fig. A2 but for a rotating fluid ($f = 10^{-4}$ s^{-1}). The solutions for the height field, h, the zonal wind, u, and the meridional wind, v, are plotted at the times $t = 0$, 1, 2, 3, 4, 5, and 6 h.

height field and speed of propagation of the surge to the west. The model tends to underestimate the velocity field at the leading edge of the surge where, however, the momentum is small.

Figure A3 displays the flow evolution for a rotating fluid ($f = 10^{-4}$ s^{-1}). The initial westward surge is Coriolis deflected to produce strong southerly flow. As a consequence of the reduction in the zonal wind, the westward advance is arrested after about 4 h when the leading edge of the flow becomes eastward.

REFERENCES

Acheson, D. J., 1990: *Elementary Fluid Dynamics.* Oxford University Press, 397 pp.

Atkins, N. T., R. M. Wakimoto, and C. L. Ziegler, 1998: Observations of the finescale structure of a dryline during VORTEX 95. *Mon. Wea. Rev.,* **126,** 525–550.

Bannon, P. R., 1983: Quasi-geostrophic frontogenesis over topography. *J. Atmos. Sci.,* **40,** 2266–2277.

Beebe, R. G., 1958: An instability line development as observed by the tornado research airplane. *J. Meteor.,* **15,** 278–283.

Benjamin, S. G., and T. N. Carlson, 1986: Some effects of surface heating and topography on the regional severe storm environment. Part I: Three-dimensional simulations. *Mon. Wea. Rev.,* **114,** 307–329.

Blackadar, A. K., 1957: Boundary layer wind maxima and their significance for the growth of nocturnal inversions. *Bull. Amer. Meteor. Soc.,* **38,** 283–290.

Bluestein, H. B., 1993: The dryline. *Synoptic–Dynamic Meteorology in Midlatitudes,* Vol. II. Oxford University Press, 282–290.

——, and S. S. Parker, 1993: Modes of isolated severe convective storm formation along the dryline. *Mon. Wea. Rev.* **121,** 1354–1372.

——, E. W. McCaul Jr., G. P. Byrd, and G. R. Woodall, 1988: Mobile sounding observations of a tornadic storm near the dryline: The Canadian, Texas storm of 7 May 1986. *Mon. Wea. Rev.,* **116,** 1790–1804.

Bonner, W. D., 1968: Climatology of the low-level jet. *Mon. Wea. Rev.,* **96,** 833–850.

——, and J. Paegle, 1970: Diurnal variations in boundary layer winds over the south-central United States in summer. *Mon. Wea. Rev.,* **98,** 735–744.

Carlson, T. N., and F. H. Ludlam, 1968: Conditions for the occurrence of severe local storms. *Tellus,* **20,** 203–226.

——, R. A. Anthes, M. Schwartz, S. G. Benjamin, and D. G. Baldwin, 1980: Analysis and prediction of severe storms environment. *Bull. Amer. Meteor. Soc.,* **61,** 1018–1032.

——, S. G. Benjamin, G. S. Forbes, and Y. F. Li, 1983: Elevated mixed layers in the regional severe storm environment: Conceptual model and case studies. *Mon. Wea. Rev.,* **111,** 1453–1473.

Chen, T. C., and J. A. Kpaeyeh, 1993: The synoptic-scale environment associated with the low-level jet of the Great Plains. *Mon. Wea. Rev.,* **121,** 416–420.

Crawford, T. M., and H. B. Bluestein, 1997: Characteristics of dryline passage during COPS-91. *Mon. Wea. Rev.,* **125,** 463–477.

Davies, H. C., 1984: On the orographic retardation of a cold front. *Contrib. Atmos. Phys.,* **57,** 409–418.

Defant, F., 1951: Local winds. *Compendium of Meteorology,* T. F. Malone, Ed., Amer. Meteor. Soc., 655–672.

Djuric, D., and M. S. Damiani Jr., 1980: On the formation of the low-level jet over Texas. *Mon. Wea. Rev.,* **108,** 1854–1865.

——, and D. S. Ladwig, 1983: Southerly low-level jet in the winter cyclones of the southwestern Great Plains. *Mon. Wea. Rev.,* **111,** 2275–2281.

Fast, J. D., and M. D. McCorcle, 1990: A two dimensional numerical sensitivity study of the Great Plains low-level jet. *Mon. Wea. Rev.,* **118,** 151–163.

Frei, C., 1993: Dynamics of a two-dimensional ribbon of shallow water on an f-plane. *Tellus,* **45A,** 44–53.

Fujita, T. T., 1958: Structure and movement of a dry front. *Bull. Amer. Meteor. Soc.,* **39,** 574–582.

Hane, C. E., C. L. Ziegler, and H. B. Bluestein, 1993: Investigation of the dryline and convective storms initiated along the dryline. Field experiments during COPS-91. *Bull. Amer. Meteor. Soc.,* **74,** 2133–2145.

Hess, S. L., 1959: *Introduction to Theoretical Meteorology.* Holt, Rhinehart and Winston, 362 pp.

Hobbs, P. V., J. D. Locatelli, and J. E. Martin, 1996: A new conceptual model for cyclones generated in the lee of the Rocky Mountains. *Bull. Amer. Meteor. Soc.,* **77,** 1169–1178.

Hoecker, W. H., Jr., 1963: Three southerly low-level jet systems delineated by the Weather Bureau special pibal network of 1961. *Mon. Wea. Rev.,* **91,** 573–582.

Holton, J. R., 1967: The diurnal boundary layer wind oscillation along sloping terrain. *Tellus,* **19,** 199–205.

Kaplan, M. L., and V. M. Karyampudi, 1992a: Meso-beta scale numerical simulations of terrain drag induced along jet stream circulations. Part I: Midtropospheric frontogenesis. *Meteor. Atmos. Phys.,* **49,** 133–156.

——, and ——, 1992b: Meso-beta scale numerical simulations of terrain drag induced along jet stream circulations. Part II: Concentration of potential vorticity within dryline bulges. *Meteor. Atmos. Phys.,* **49,** 157–185.

Keyser, D., and T. N. Carlson, 1984: Transverse ageostrophic circulations associated with elevated mixed layers. *Mon. Wea. Rev.,* **112,** 2465–2478.

Kovacs, T. A., 1996: Diurnal variation in the movement and structure of the quiescent dryline. M.S. thesis, Dept. of Meteorology, The Pennsylvania State University, 81 pp.

——, and P. R. Bannon, 1997: An air mass frontal model of the dryline. Preprints, *11th Conf. on Atmospheric and Oceanic Fluid Dynamics,* Tacoma, WA, Amer. Meteor. Soc., 91–94.

Kuo, A. C., and L. M. Polvani, 1997: Time-dependent fully nonlinear geostrophic adjustment. *J. Phys. Oceanogr.,* **27,** 1614–1634.

Lanicci, J. M., and T. T. Warner, 1991a: A synoptic climatology of the elevated mixed-layer inversion over the southern Great Plains in spring. Part I: Structure, dynamics, and seasonal evolution. *Wea. Forecasting,* **6,** 181–197.

——, and ——, 1991b: A synoptic climatology of the elevated mixed-layer inversion over the southern Great Plains in spring. Part II: The life cycle of the lid. *Wea. Forecasting,* **6,** 198–213.

——, and ——, 1991c: A synoptic climatology of the elevated mixed-layer inversion over the southern Great Plains in spring. Part III: Relationship to severe-storms climatology. *Wea. Forecasting,* **6,** 214–226.

Martin, J. E., J. D. Locatelli, P. V. Hobbs, P.-Y. Wang, and J. A. Castle, 1995: Structure and evolution of winter cyclones in the central United States and their effects on the distribution of precipitation. Part I: A synoptic-scale rainband associated with a dryline and lee trough. *Mon. Wea. Rev.,* **123,** 241–264.

McCarthy, J., and S. E. Koch, 1982: The evolution of an Oklahoma dryline. Part I: A meso- and subsynoptic-scale analysis. *J. Atmos. Sci.,* **39,** 225–236.

McGuire, E. L., 1962: The vertical structure of three drylines as revealed by aircraft traverses. NSSP Reprint 7, U.S. Weather Bureau, 10 pp. [Available from P. R. Bannon, Dept. of Meteorology, The Pennsylvania State University, University Park, PA 16802.]

McNider, R. T., and R. A. Pielke, 1981: Diurnal boundary-layer development over sloping terrain. *J. Atmos. Sci.,* **38,** 2198–2212.

——, and F. J. Kopp, 1990: Specification of the scale and magnitude of thermals used to initiate convection in cloud models. *J. Appl. Meteor.,* **29,** 99–104.

Miller, J. A., 1998: A comparison of diurnal motion theories for the quiescent dryline using a shallow water model. M.S. thesis, Dept. of Meteorology, The Pennsylvania State University, 66 pp.

Mitchell, M. J., R. W. Arritt, and K. Labor, 1995: A climatology of the warm season Great Plains low-level jet using wind profiler observations. *Wea. Forecasting,* **10,** 576–591.

NSSP Staff Members, 1963: Environmental and thunderstorm structures as shown by National Severe Storms Project observations in spring 1960 and 1961. *Mon. Wea. Rev.,* **91,** 271–292.

Paegle, J., and G. E. Rasch, 1973: Three-dimensional characteristics of diurnally varying boundaries layer flows. *Mon. Wea. Rev.,* **101,** 746–756.

Parish, T. R., A. R. Rodi, and R. D. Clark, 1988: A case study of the summertime Great Plains low-level jet. *Mon. Wea. Rev.,* **116,** 94–105.

Parsons, D. B., M. A. Shapiro, M. Hardesty, R. J. Zamora, and J. M. Intrieri, 1991: The finescale structure of a west Texas dryline. *Mon. Wea. Rev.,* **119,** 1242–1258.

Rhea, J. O., 1966: A study of thunderstorm formation along drylines. *J. Appl. Meteor.,* **5,** 58–63.

Schaefer, J. T., 1973: The motion of the dryline. Preprints, *Eighth Severe Storm Conf.,* Denver, CO, Amer. Meteor. Soc., 104–107.

——, 1974a: A simulative model of dryline motion. *J. Atmos. Sci.,* **31,** 956–954.

——, 1974b: The life cycle of the dryline. *J. Appl. Meteor.,* **13,** 444–449.

——, 1986: The dryline. *Mesoscale Meteorology and Forecasting,* P. S. Ray, Ed., Amer. Meteor. Soc., 549–572.

Schär, C., and R. B. Smith, 1993: Shallow-water flow past isolated topography. Part I: Vorticity production and wake formation. *J. Atmos. Sci.,* **50,** 1373–1400.

——, and P. K. Smolarkiewicz, 1996: A synchronous and iterative flux-correction formalism for coupled transport equations. *J. Comput. Phys.,* **128,** 101–120.

Smolarkiewicz, P. K., and L. G. Margolin, 1993: On forward-in-time differencing for fluids: Extension to a curvilinear framework. *Mon. Wea. Rev.,* **121,** 1847–1859.

Steenburgh, W. J., and C. F. Mass, 1994: The structure and evolution of a simulated Rocky Mountain lee trough. *Mon. Wea. Rev.,* **122,** 2740–2761.

Stull, R. B., 1988: *An Introduction to Boundary Layer Meteorology.* Kluwer Academic, 666 pp.

Sun, W. Y., 1987: Mesoscale convection along the dryline. *J. Atmos. Sci.,* **44,** 1394–1403.

——, and Y. Ogura, 1979: Boundary layer forcing as a possible trigger to a squall line formation. *J. Atmos. Sci.,* **36,** 235–254.

——, and C. C. Wu, 1992: Formation and diurnal variation of the dryline. *J. Atmos. Sci.,* **49,** 1606–1619.

Tepper, M., 1955: On the generation of pressure-jump lines by the impulsive addition of momentum to simple current systems. *J. Meteor.,* **12,** 287–297.

Uccellini, L. W., 1980: On the role of upper tropospheric jet streaks and leeside cyclogenesis in the development of low-level jets in the Great Plains. *Mon. Wea. Rev.,* **108,** 1689–1696.

Wakimoto, R. M., W. C. Lee, H. B. Bluestein, C. H. Liu, and P. H. Hildebrand, 1996: ELDORA observations during VORTEX 95. *Bull. Amer. Meteor. Soc.,* **77,** 1465–1481.

Wexler, H., 1961: A boundary layer interpretation of the low-level jet. *Tellus,* **13,** 369–378.

Ziegler, C. L., and C. E. Hane, 1993: An observational study of the dryline. *Mon. Wea. Rev.,* **121,** 1134–1151.

——, and E. N. Rasmussen, 1998: The initiation of moist convection at the dryline: Forecasting issues from a case study perspective. *Wea. Forecasting,* **13,** 1106–1131.

——, W. J. Martin, R. A. Pielke, and R. L. Walko, 1995: A modeling study of the dryline. *J. Atmos. Sci.,* **52,** 263–285.

——, T. J. Lee, and R. A. Pielke Sr., 1997: Convective initiation at the dryline: A modeling study. *Mon. Wea. Rev.,* **125,** 1001–1026.